LEGIBILITY NOTICE

A major purpose of the Technical Information Center is to provide the broadest dissemination possible of information contained in DOE's Research and Development Reports to business, industry, the academic community, and federal, state and local governments.

Although a small portion of this report is not reproducible, it is being made available to expedite the availability of information on the research discussed herein.

LA-UR 89-1593

CONF-8903121

Received by OSTI

JUN 07 1989

TITLE The Magnetic Topology of the Plasmoid Flux Rope in a MHD Simulation of Magnetotail Reconnection

LA-UR--89-1593

DE89 012621

AUTHOR(S) J. Birn and M. Hesse

SUBMITTED TO Proceedings of the Chapman Conference on the Physics of Magnetic Flux Ropes, Hamilton, Bermuda, 27-31 March 1989

Los Alamos

Los Alamos National Laboratory
Los Alamos, New Mexico 87545

The Magnetic Topology of the Plasmoid Flux Rope in a MHD Simulation of Magnetotail Reconnection

J. Birn and M. Hesse

University of California, Los Alamos National Laboratory, Los Alamos, NM 87545

Abstract. On the basis of a three-dimensional MHD simulation we discuss the magnetic topology of a plasmoid that forms by a localized reconnection process in a magnetotail configuration including a net dawn-dusk magnetic field component B_{yN}. As a consequence of $B_{yN} \neq 0$ the plasmoid gets a helical flux rope structure rather than an isolated island or bubble structure. Initially all field lines of the plasmoid flux rope remain connected with the Earth, while at later times a gradually increasing amount of flux tubes becomes separated, connecting to either the distant boundary or to the flank boundaries. In this stage topologically different flux tubes become tangled and wrapped around each other, consistent with predictions on the basis of ad-hoc plasmoid models.

Introduction

One of the major components of the common model of magnetotail activity, associated with magnetospheric substorms, is the severance, and subsequent tailward ejection, of a part of the plasma sheet, called the plasmoid [e.g., *Hones*, 1977]. The simplest picture of the magnetic topology and of its changes during this process, guided by two-dimensional or symmetric models, is that the plasmoid represents a magnetic "bubble," an entity consisting of closed loops of field lines, formed from closed plasma sheet field lines through magnetic reconnection, and enclosed by a magnetic flux surface. It has been realized, however, that the picture where field lines reconnect with themselves to form closed loops is highly singular and requires a symmetry that will usually not exist [*Hughes and Sibeck*, 1987; *Schindler et al.*, 1988; *Birn et al.*, 1989]. The more general picture of a plasmoid involves helical field lines rather than closed loops, which must be connected with either the Earth or interplanetary space and thus form a flux rope of field lines, not necessarily topologically different from the usual plasma sheet, lobe, or open field lines.

In the present paper we will investigate the structure of such a plasmoid flux rope, found in a 3-D MHD simulation of magnetic reconnection in the Earth's magnetic tail. A companion paper [*Hesse and Birn*, 1989] addresses the properties of the electric field in this simulation, with the emphasis on the component parallel to the magnetic field and on possible acceleration effects. An extended discussion of the simulation is given by *Birn and Hesse* [1989]. An understanding of the particular structure of the plasmoid flux rope, developing in a self-consistent way, might also help to understand and interpret apparent flux rope structures in other space environments, such as the magnetopause (flux transfer events), the solar atmosphere, the solar wind, or other planetary environments.

Field Evolution and Magnetic Topology

The simulation started from a magnetotail equilibrium configuration (Figure 1) that includes a net dawn-dusk magnetic field component, B_{yN}, which breaks the mirror symmetry around the center plane $z = 0$ of the plasma sheet [*Birn*, 1989]. Additional features of the initial equilibrium, already included in earlier simulations [*Birn and Hones*, 1981; *Birn*, 1984], are gradients in the x direction, i.e., along the tail axis, associated with a field component, B_z, normal to the plasma/current sheet, and an increase of B_z, and accordingly of the plasma sheet thickness, away from the center of the tail toward the dawn and dusk flanks ($\pm y$ directions). Further details of the initial configuration are given by *Birn and Hesse* [1989] and *Birn* [1989].

The dynamic evolution of the tail was initiated by imposing finite resistivity, which allowed an unstable tearing mode to develop from an initial diffusion. For simplicity, and to avoid the prescription of the location and extent of the reconnection region, the resistivity η was chosen constant, corresponding to a Lundquist number $S = \mu_0 L_c V_c/\eta = 200$, where L_c represents a typical scale length (current sheet half width) in the z direction, and V_c is a typical MHD wave speed, that is here, an Alfvén speed, defined by the characteristic lobe magnetic field strength and the plasma sheet density. The magnitude of the net cross-tail field component B_{yN} was chosen to be about 3% of the lobe field, consistent with average observed data [*Fairfield*, 1979]. For comparison, a symmetric case with $B_{yN} = 0$ was also studied.

Figure 2 shows the magnetic field evolution in the midnight meridian plane $y = 0$. The lines are trajectories of the vector field B_x, B_z only and not magnetic field lines or projections of field lines. Due to the smallness of B_y, and in particular of $\partial B_y/\partial y$, however, the shown configuration is very close to the case $B_{yN} = 0$, so that Figure 2 is almost identical with the corresponding figure in that case, where the lines shown would represent actual field lines. The field evolution exhibited by Figure 2 indicates the formation of a plasmoid and its tailward ejection found already in earlier simulations [e.g., *Birn and Hones*, 1981].

The southward turning of B_z in the equatorial plane, which marks the formation of a neutral line and of a plasmoid in the symmetric case $B_{yN} = 0$, occurs at about $t = 100$, where the time is normalized by a characteristic Alfvén crossing time. The results demonstrated by Figure 2 confirm that the field evolution is not significantly altered by the presence of the net B_y, so that it seems reasonable to continue the terminology "plasmoid formation and motion," developed on the basis of the symmetric case.

The magnetic field topology, however, is altered by the presence of the net B_y, which does not drastically change in the reconnection region during the evolution [*Birn and Hesse*, 1989]. Instead of an isolated magnetic bubble we find indeed a magnetic flux rope, consisting of helical field lines, that are initially still connected with the Earth at both ends, but open this connection at later times (see Figures 3–5). Since plasmoid field lines are not topologically different from other field lines in a strict sense, we have used a pragmatic criterion to identify the plasmoid. Plasmoid field lines are defined as field lines that cross the neutral sheet, identical with the equatorial plane $z = 0$ in our case, more than once. This criterion picks out typical helical field lines. It is not a strict topological criterion, however, because it is based on the arbitrary choice of a certain plane. Figure 3 shows, in a perspective view, four field lines at $t = 165$. One of these (labeled b) belongs to the plasmoid according to our criterion. One (labeled a) belongs to the plasmasheet earthward of the reconnection region, and the other one (labeled d) belongs to the plasmasheet tailward from the plasmoid, which is not affected yet by the reconnection process. Both of these field lines cross the equatorial plane only once and can thereby be distinguished from the plasmoid field lines. The fourth field line (labeled c) crosses the equatorial plane also only once, due to its small pitch; it belongs therefore formally not to the plasmoid. Since it is located inside the region of plasmoid field lines with the major part of the plasmoid field lines winding around it, however, it should be considered as such a field line, too. This shows the problems with a criterion that is not based on the properties of the magnetic field only. Fortunately only very few field line are affected by this classification problem in the present case.

A perspective view of the apparent plasmoid flux rope surface is given by Figures 4 and 5 for two different times. The flux rope represented in these figures is not only twisted, but also folded, so that field lines that are near the apparent surface in one region may become apparent interior field lines in another region. This is more obvious at the later time (Fig. 5), when the plasmoid consists not only of closed field lines, that are connected with the Earth at both ends, but also of open field lines connecting the earthward boundary $x = 0$ with the distant boundary $x = -60$ (heavily shaded bundle) or with the flank boundaries $|y| = 10$ (lightly shaded bundles) (all lengths normalized by L_c, the characteristic plasma sheet scale length in the z direction (current sheet half thickness) nearest to the Earth). A closed field line starting near the outer plasmoid surface on one side of the tail may end near the interior surface between open and closed field lines on the other side. Figure 5 shows how flux tubes with different connections get intertwined and wrapped around each other as predicted by *Birn et al.* [1989] on the basis of an ad hoc 3-D plasmoid model. Note that, despite the smallness of B_y, most field lines make only a few loops around the center of the plasmoid flux rope, as one can see from Figures 3–5. The reason is the large size of the plasmoid in the x direction, which leads to a considerable displacement of a field line in the y direction despite the smallness of B_y.

From Figure 5 it may look as if the amount of open plasmoid flux connected with the flank boundaries is comparable to, or even larger than the open plasmoid flux connected to the distant boundary. This, however, is misleading. The amount of flux connected to the flanks is in fact much smaller than the amount connected to the distant boundary, despite comparable surface areas at the boundaries, because the former one carries only the small B_y component across the boundary, while the distant flux carries the much larger B_x component across. This is the reason why only open plasmoid flux connected with the distant boundary (dark shading) is visible at the near-earth boundary in Figure 5.

The detailed internal structure of the plasmoid and its evolution are further demonstrated by Figure 6, which shows the magnetic connections in several cross-sections $x = const$ of the tail at $t = 212$. The different types of field lines are indicated by different symbols as explained in the figure caption. The figure demonstrates again the complexity of the field connections in the later stage, when the plasmoid separates from Earth. Surprisingly, this separation starts much later than suggested by Figure 2.

For comparisons with observations of a plasmoid in the magnetotail or with other apparent flux rope structures in space, it is of particular interest to study the temporal variation of field components at a fixed location. This is done in Figures 7 and 8, which show the evolution of the three components of the magnetic field in the midnight meridian plane $y = 0$ for $z = 0$ and $z = 0.56$, repectively, and the locations $x = -30$ and $x = -45$. The locations in x are tailward from the reconnection site near $x = -10$ at distances corresponding to about 40 R_E and 70 R_E, if we assume a scaling length $L_c = 2$ R_E. Note that in our present simulation both locations are still within the initially closed plasma sheet region, where B_z is positive before the passage of the plasmoid. Both figures show how the north-south signature of the passing plasmoid becomes more pronounced with distance. The B_y components show also a maximum-minimum signature with a small phase delay against the north-south signature of B_z. The first maximum is not very pronounced at the nearer location in x. There is, however, a second maximum at the locations $x = -30$, which is not, or not yet, visible at $x = -45$. The B_x component shows at all locations a minimum, that coincides with the first maximum of B_y, except at $x = -45$, $z = 0.56$. At this location B_x continues to decrease and even reverses sign. This signature, which would commonly be interpreted as a neutral sheet crossing, is related to the indented magnetic field structure in the rear end of the plasmoid at late times, visible in the last panel of Figure 2.

Summary

We have discussed the magnetic topology of a three-dimensional plasmoid, using results from a resistive MHD simulation of magnetic reconnection in the magnetotail. Due to the presence of a net dawn-dusk magnetic field component B_{yN} the plasmoid forms a flux rope with initially both feet at the near-earth boundary. As the plasmoid moves tailward, an increasing amount of flux bundles opens to the tailward boundary and, to a smaller amount, to the flank boundaries. These open flux bundles are intertwined with the closed flux bundles, that are still fully connected with the earthward boundary. Despite the smallness

of B_y the plasmoid field lines exhibit typically only a few loops, before they return to Earth or to the distant tail. The reason is the large size of the plasmoid in the x direction, i.e., along the tail, compared to its dawn-dusk extent. The plasmoid flux rope is not only twisted, but also folded, so that field lines that are located near its apparent surface in one region can become apparent interior field lines in another region.

Acknowledgments. This work was supported by the U.S. Department of Energy through the Office for Basic Energy Sciences and by NASA under contract W-7405-ENG-36. M. H. gratefully acknowledges support from the Los Alamos National Laboratory Director's postdoctoral program.

References

Birn, J., Three-dimensional computer modeling of dynamic reconnection in the magnetotail, in *Magnetic Reconnection in Space and Laboratory Plasmas, Geophys. Monogr. Ser.*, vol. 30, edited by E. W. Hones, Jr., p. 264, AGU, Washington, D. C., 1984.

Birn, J., The distortion of the magnetotail equilibrium structure by a net cross-tail magnetic field, *J. Geophys. Res.*, submitted 1989.

Birn, J., and M. Hesse, MHD simulations of magnetic reconnection in a skewed three-dimensional tail configuration, *J. Geophys. Res.*, submitted 1989.

Birn, J. and E. W. Hones, Jr., Three-dimensional computer modeling of dynamic reconnection in the geomagnetic tail, *J. Geophys. Res.*, *86*, 6802, 1981.

Birn, J., M. Hesse, and K. Schindler, Filamentary structure of a three-dimensional plasmoid, *J. Geophys. Res.*, *94*, 252, 1989.

Fairfield, D. H., On the average configuration of geomagnetic tail, *J. Geophys. Res.*, *84*, 1950, 1979.

Hesse, M., and J. Birn, Parallel electric fields in a simulation of magnetotail reconnection and plasmoid evolution, this issue.

Hones, E. W., Jr., Substorm processes in the magnetotail: Comments on 'On hot tenuous plasma fireballs and boundary layers in the Earth's magnetotail' by L. A. Frank, L. L. Ackerson, and R. P. Lepping, *J. Geophys. Res.*, *82*, 5633, 1977.

Hughes, W. J., and D. G. Sibeck, On the 3 dimensional structure of plasmoids, *Geophys. Res. Lett.*, *14*, 636, 1987.

Schindler, K., M. Hesse, and J. Birn, General magnetic reconnection, parallel electric fields, and helicity, *J. Geophys. Res.*, *93*, 5547, 1988.

Figure Captions

Fig. 1. Perspective view of the initial configuration as seen from the tail, showing a magnetic flux surface, originating from a circle $r = 20$ R_E at $X_{GSM} = -20$ R_E. The shaded region consists of field lines with both ends inside this circle.

Fig. 2. Magnetic field evolution in the midnight meridian plane $y = 0$. The lines connect projections of field vectors in this plane and are not field lines or projections of field lines.

Fig. 3. Perspective view of four field lines as seen from the earthward side, for $t = 165$. Field lines labeled (a) and (d) represent ordinary plasmasheet field lines, crossing the equatorial plane just once; the field line labeled (b) represens aclosed plasmoid field line, also connected with the near-earth boundary at both ends, but crossing the equatorial plane more than once; the field line labeled (c) near the center of the plasmoid flux rope, crosses the equatorial plane only once, due to its small pitch, but should also be considered as a plasmoid field line.

Fig. 4. Perspective view of the apparent plasmoid flux rope surface as seen from the earthward side, for $t = 165$.

Fig. 5. Same as Figure 3, but for $t = 212$. Dark shading indicates open plasmoid field lines connecting the near-earth boundary $x = 0$ with the distant boundary $x = -60$; light shading indicates plasmoid field lines connected with one of the flank boundaries at $|y| = 10$.

Fig. 6. Topological connections of field lines in different planes $x = const$ for $t = 212$. The symbols represent closed plasmasheet field lines (horizontal bars), crossing the neutral sheet $z = 0$ just once; closed plasmoid field lines (symbol #), also with both ends at the near-earth boundary, but crossing the neutral sheet more than once; lobe field lines (astericks), that do not cross the neutral sheet; lobe-like plasmoid field lines (symbol X), also connecting the near-earth boundary $x = 0$ with the distant boundary $x = -60$, but with two or more neutral sheet crossings; and boundary field lines (vertical bars) connected with one of the boundaries at $|y| = 10$.

Fig. 7. Evolution of the three magnetic field components B_x, B_y, and B_z at fixed points with the coordinates $y = 0$, $z = 0$, and $x = -30$ (solid line), $x = -45$ (dashed line).

Fig. 8. Same as Figure 7, but for $z = 0.56$.

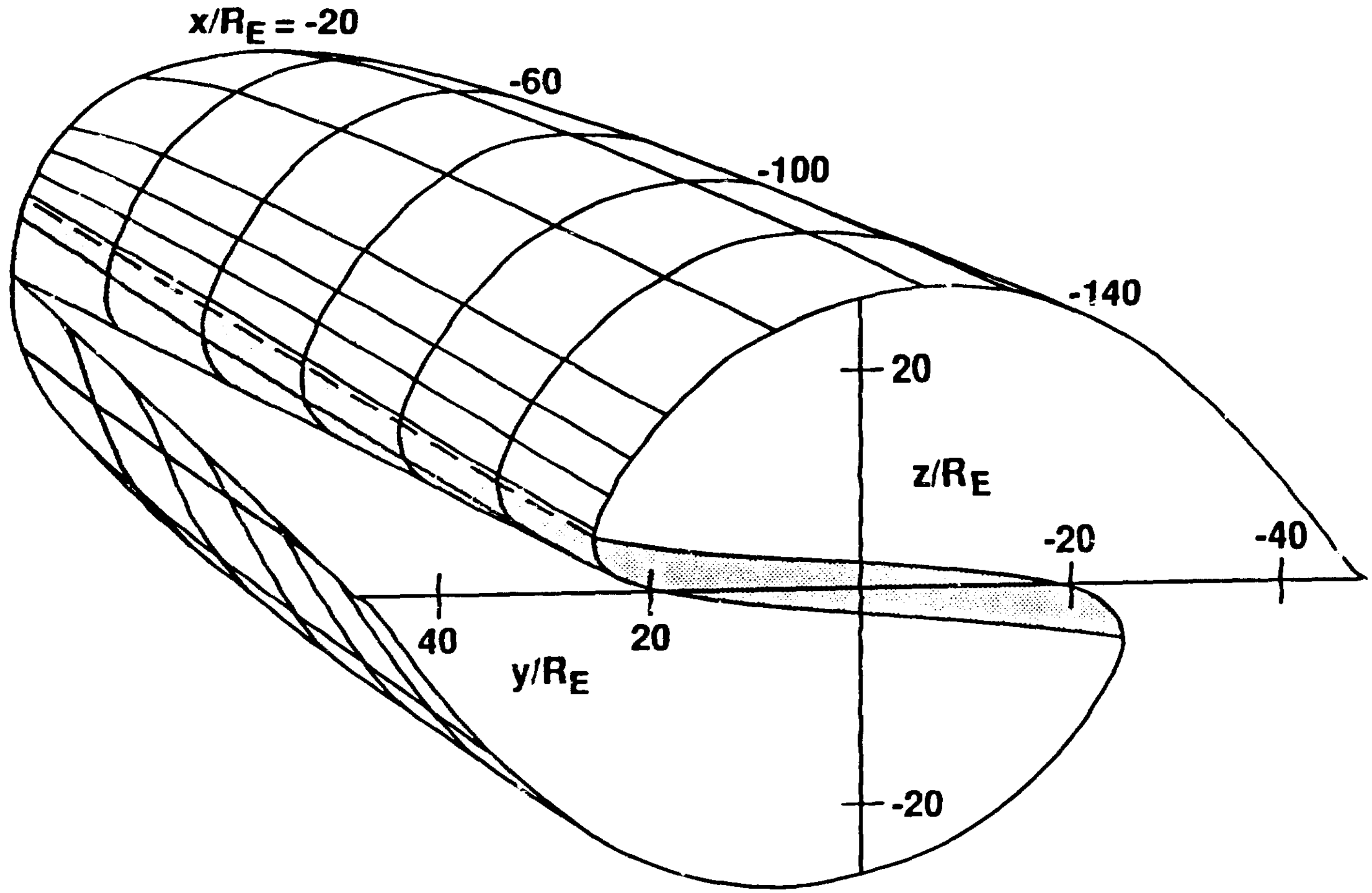

Fig. 1

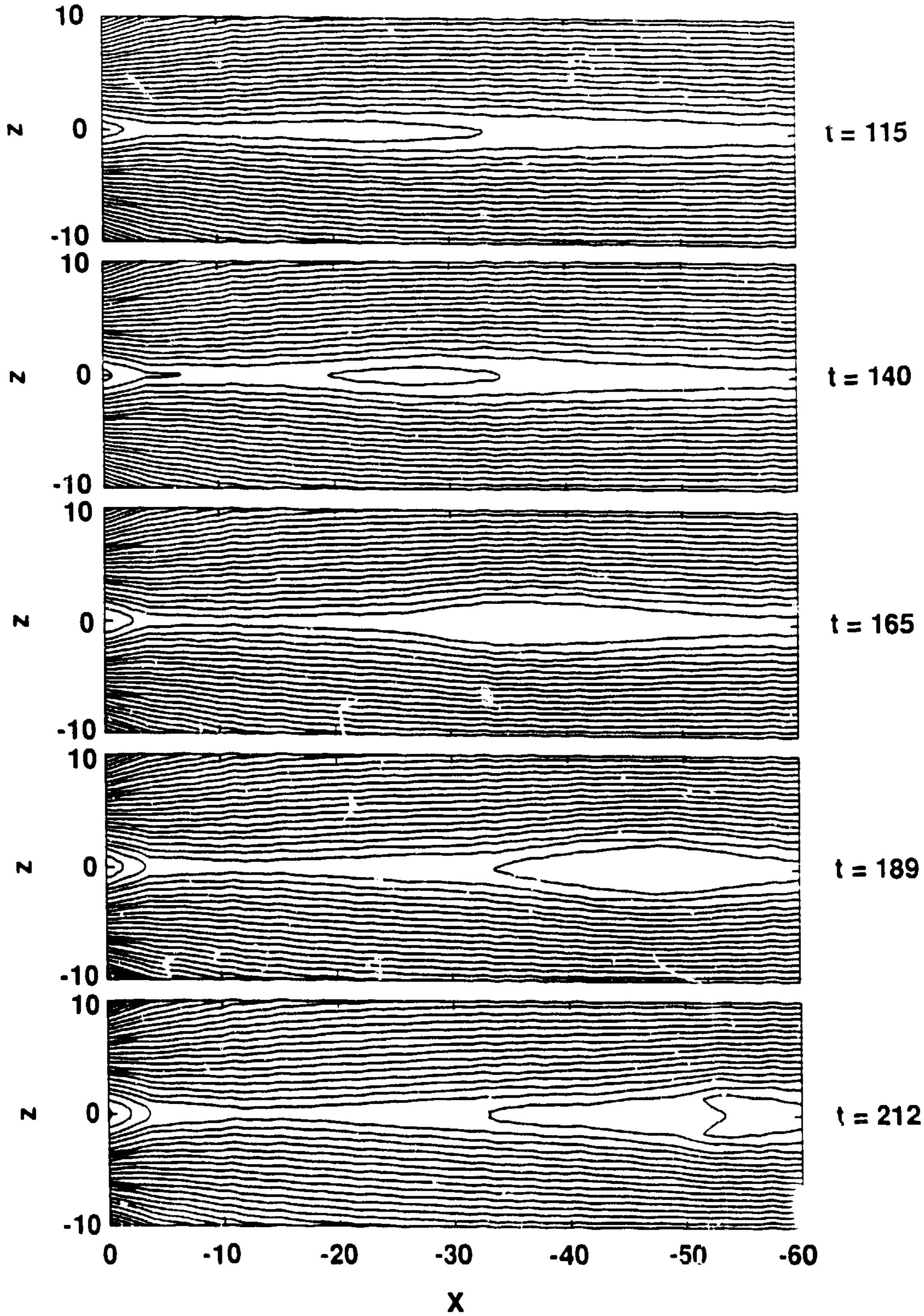

Fig. 2

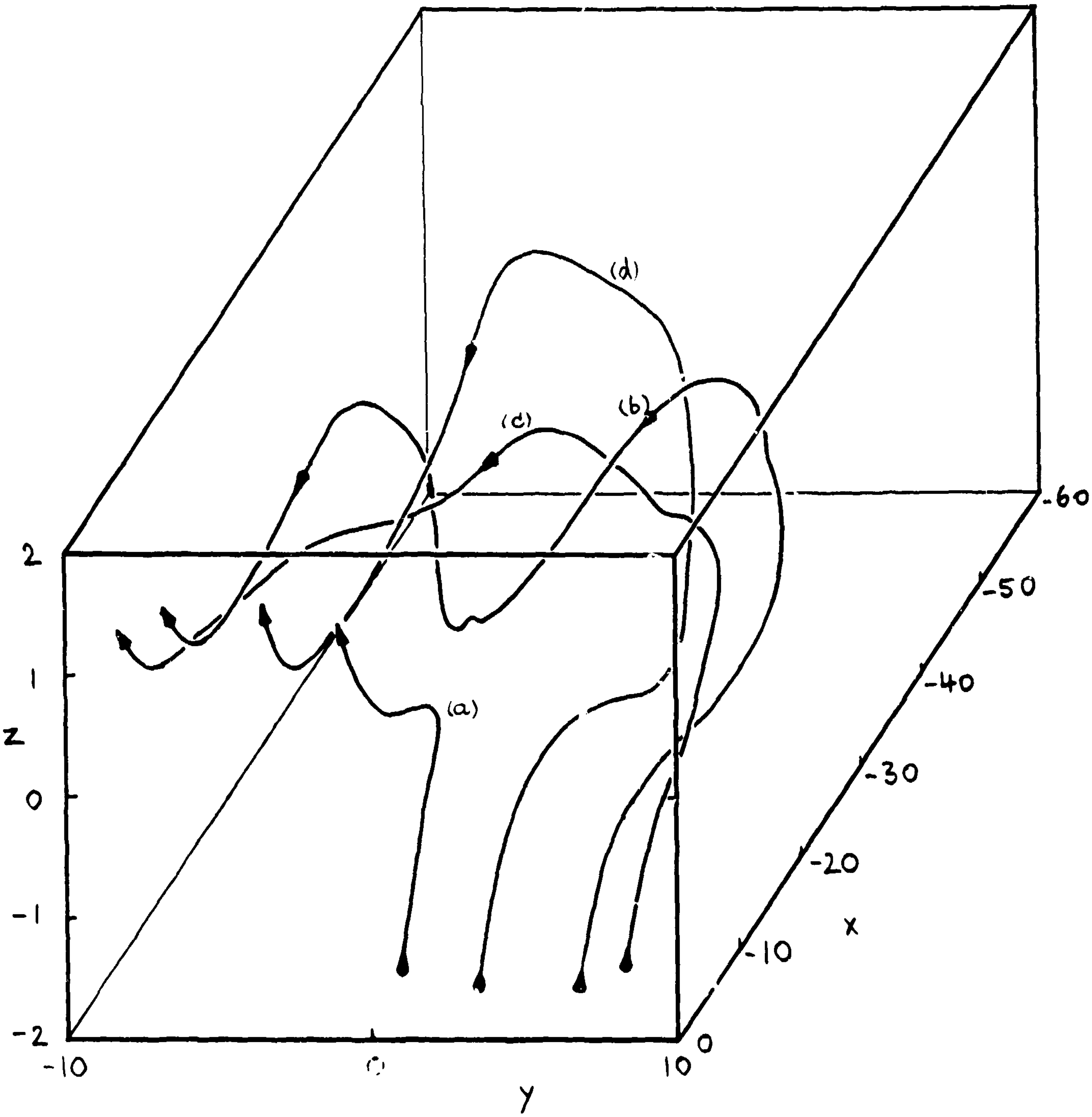

Fig. 3

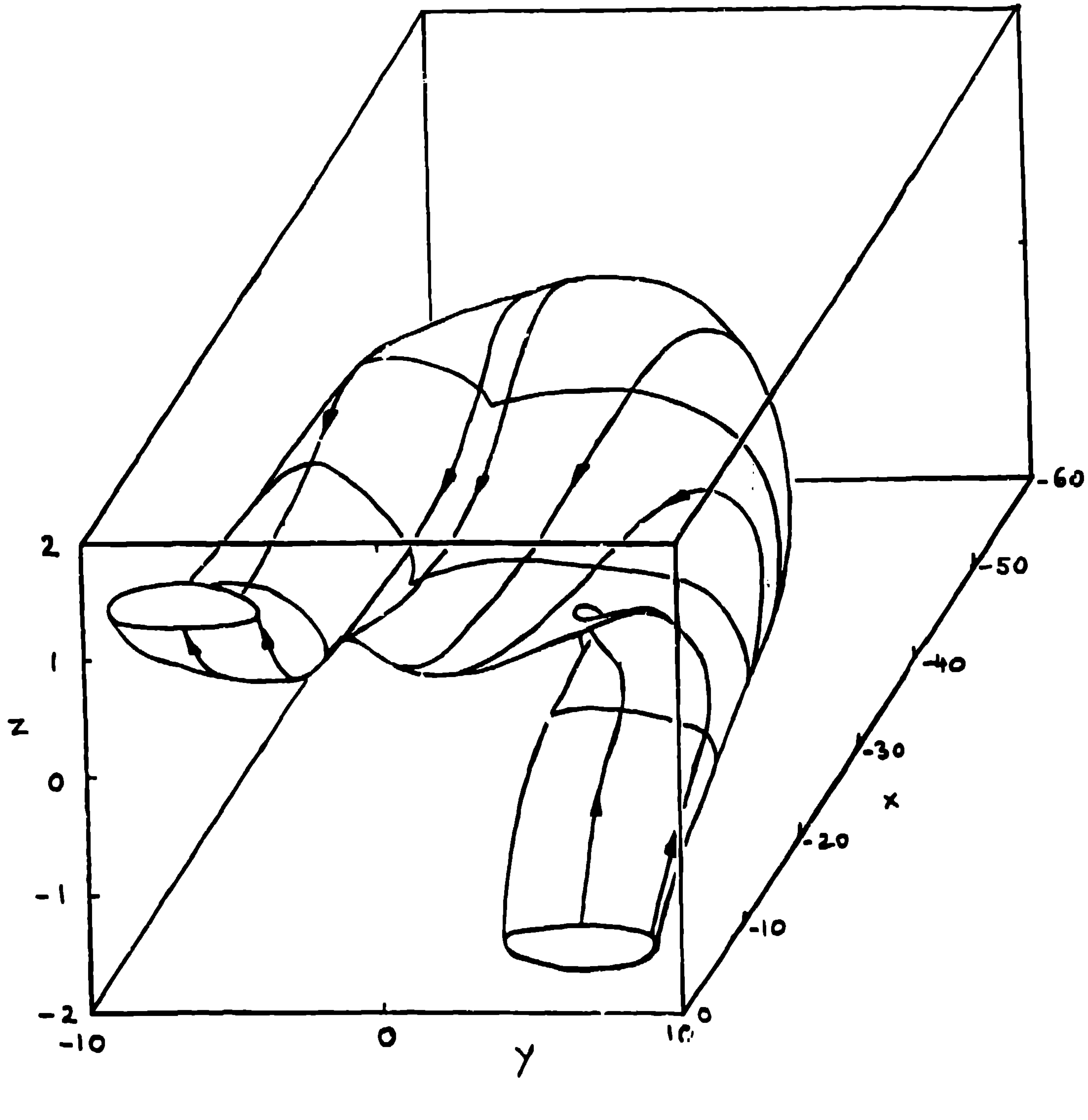
2
1
z
0
-1
-2
-10
0
y
10
0
-10
-20
-30
x
-40
-50
-60

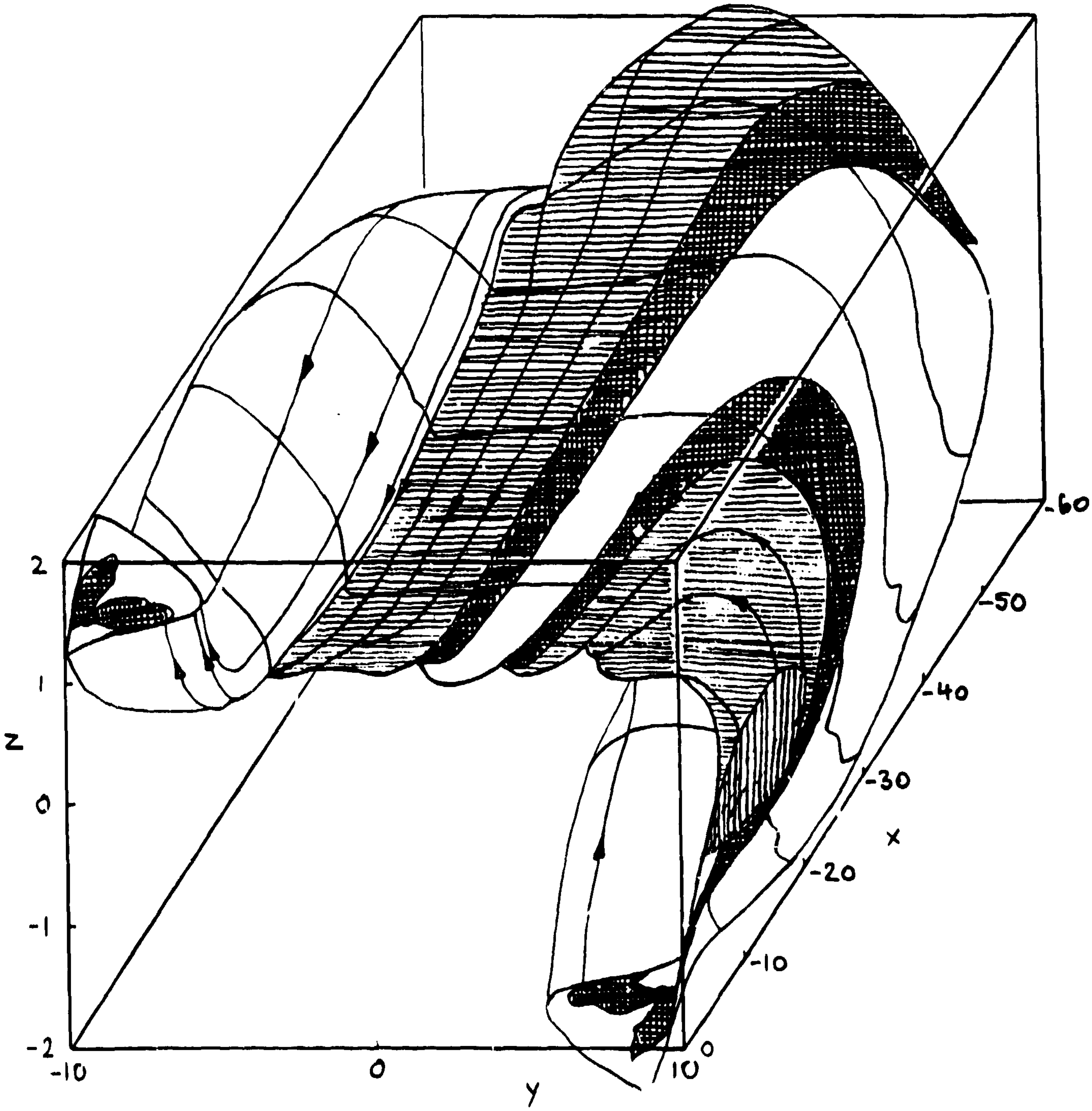

Fig. 5

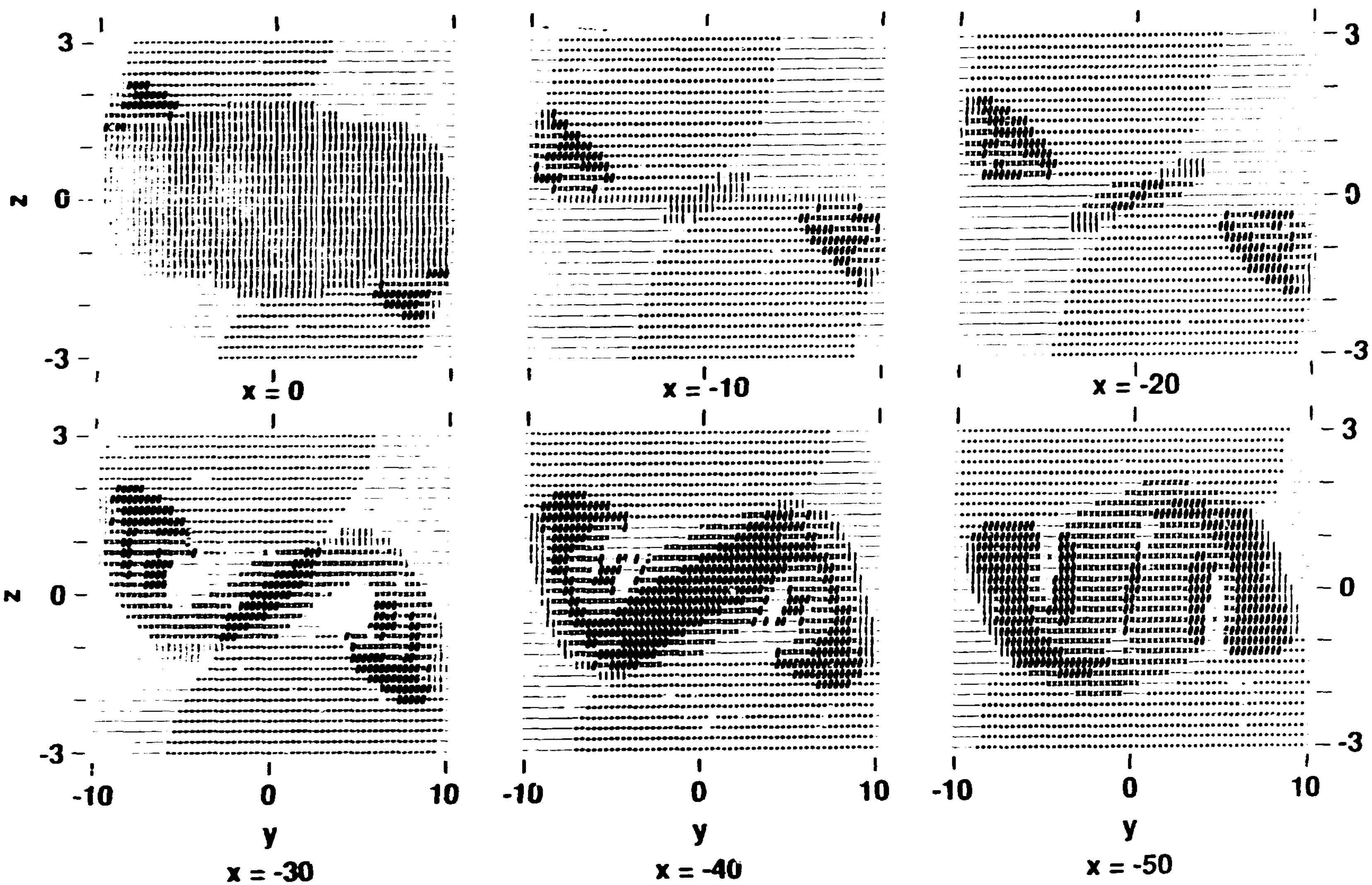

Fig. 6

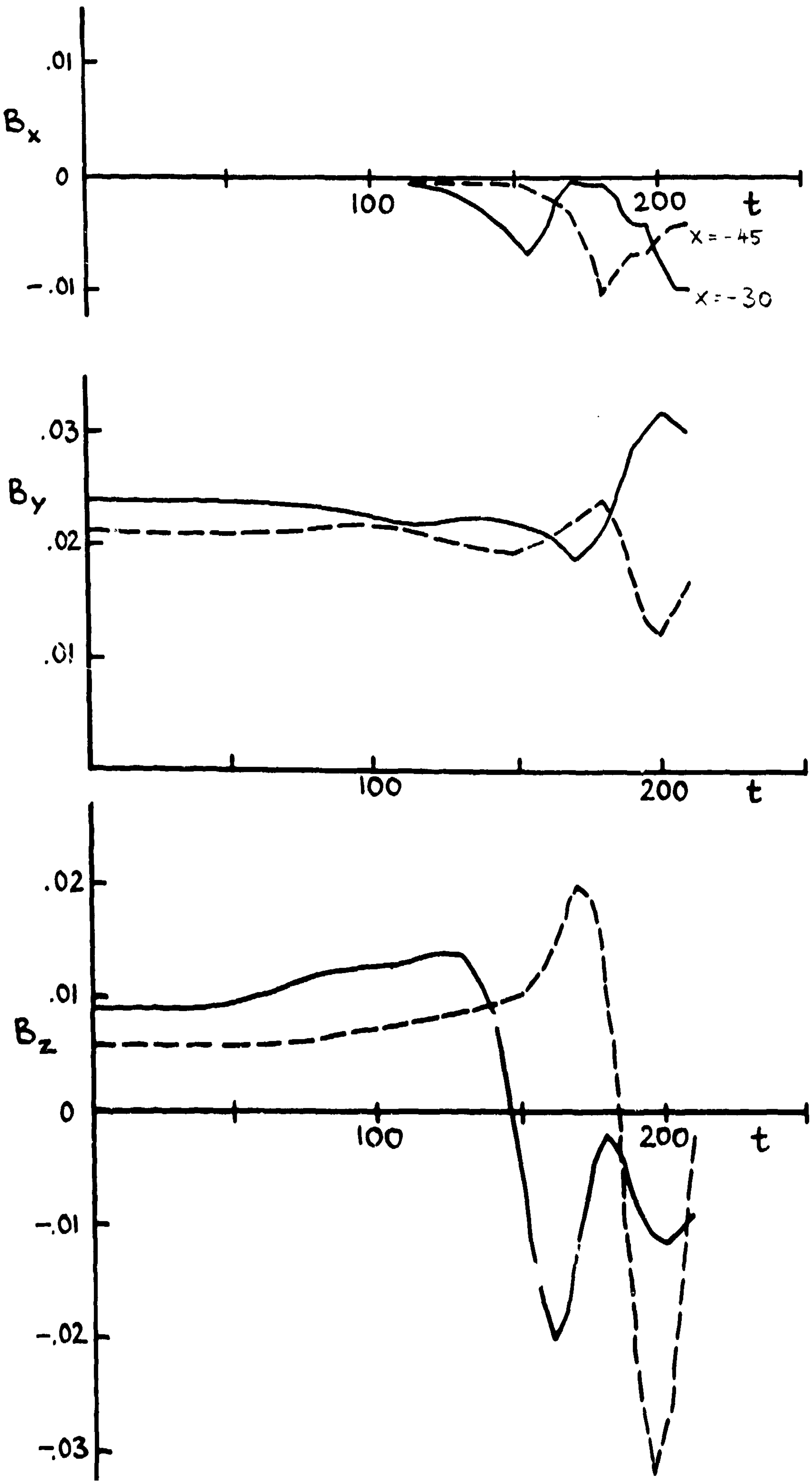
.01
B_x
0
100
200
t
x = -45
-.01
x = -30
.03
B_y
.02
.01
100
200
t
.02
.01
B_z
0
100
200
t
-.01
-.02
-.03

Fig. 7

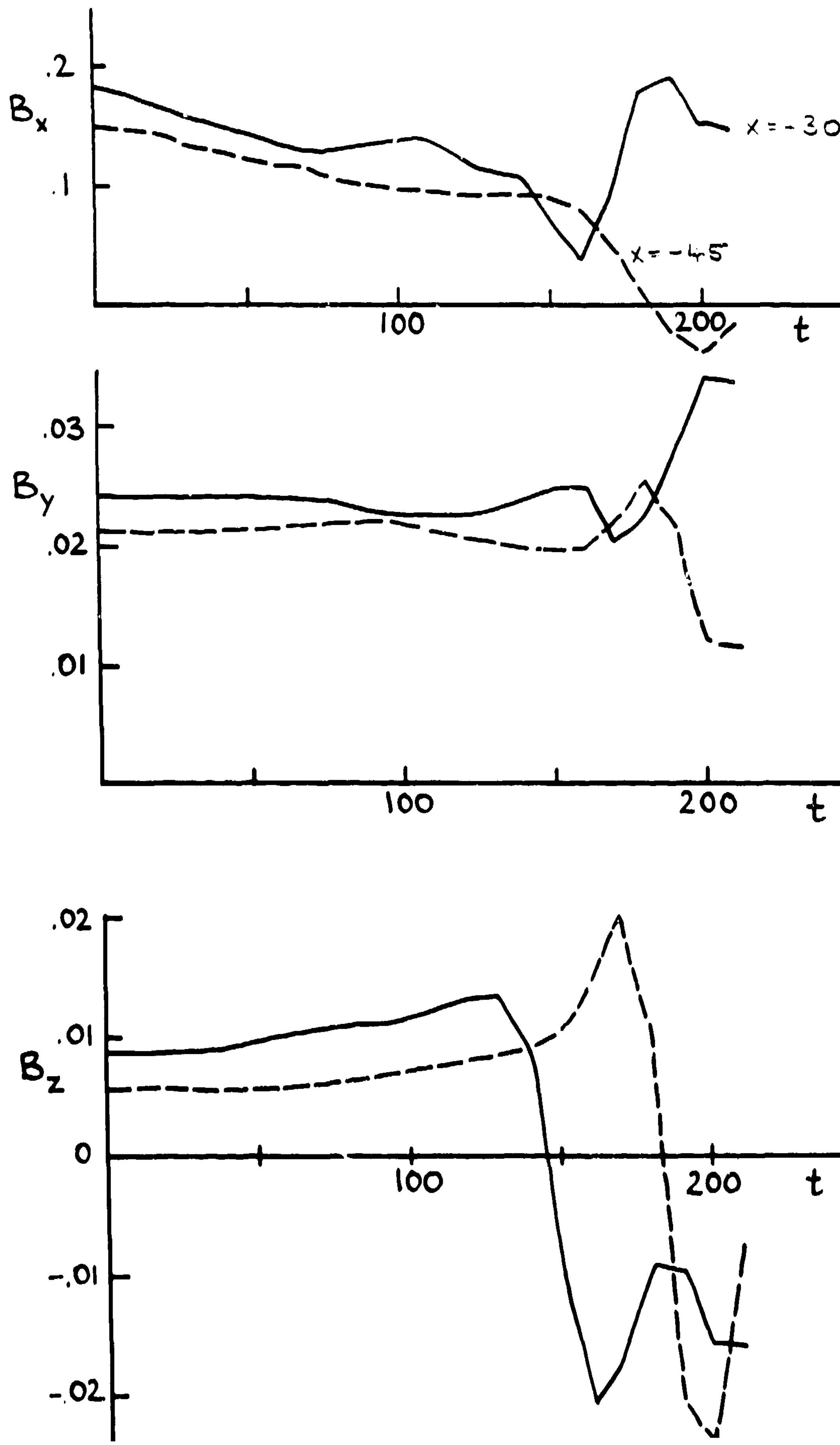
.2
B_x
.1
100
200
t
x=-30
x=-45
.03
B_y
.02
.01
100
200
t
.02
.01
B_z
0
100
200
t
-.01
-.02

Fig. 8